AUTOMATIC GENERATION OF LISSAJOUS–TYPE LIBRATION POINT TRAJECTORIES AND ITS MANIFOLDS FOR LARGE ENERGIES

Josep M. Mondelo[(1)], **Esther Barrabés**[(2)], **Gerard Gómez**[(3)], **Mercè Ollé**[(4)]

[(1)]IEEC & Departament de Matemàtiques, Universitat Autònoma de Barcelona
08193 Bellaterra (Cerdanyola del Vallès) Barcelona, Spain
e–mail: jmm@mat.uab.es

[(2)]Departament d'Informàtica i Matemàtica Aplicada, Universitat de Girona
Campus Montilivi, edifici P-IV, c/Lluís Santaló s/n, 17071 Girona, Spain
e–mail: barrabes@ima.udg.es

[(3)]IEEC & Departament de Matemàtica Aplicada i Anàlisi, Universitat de Barcelona
Gran Via 585, 08007 Barcelona, Spain
e–mail: gerard@maia.ub.es

[(4)]Departament de Matemàtica Aplicada I, Universitat Universitat Politècnica de Catalunya,
E.T.S.E.I.B., Diagonal 647, 08028 Barcelona, Spain
e–mail: merce.olle@upc.edu

ABSTRACT

In this paper we present a methodology for the automatic generation of trajectories within the Lissajous family of 2D invariant tori around L_1 of the Spatial, Circular Restricted Three–Body Problem for the Earth–Moon mass ratio. This methodology is based on the computation of a mesh of orbits which, using interpolation strategies, gives an accurate quantitative representation of the full set of libration point orbits. This representation, when combined with the one obtained using Poincaré maps, provides a useful tool for the design of missions to the libration points fulfilling specific requirements. The same methodology applies to stable and unstable manifolds as well. As an application, a representative set of the interpolated orbits is refined to a full Solar System model based on the JPL DE403 ephemeris file.

1. INTRODUCTION

The last 30 years have produced an explosion in the capabilities of designing and managing libration point missions [2]. The starting point was the third International Sun-Earth Explorer spacecraft (ISEE–3) which was launched in 1978, to the vicinity of the Sun–Earth L_1 Lagrange point, to pursue studies of the Earth-Sun interactions in a first step of what now is known as Space Weather [3]. Since 1978, interest in the scientific advantages of the Lagrange libration points for space missions has continued to increase and to inspire even more challenging objectives that are reflected, in part, in missions such as SOHO, MAP and Genesis [8]. Also, increasing understanding of the available mission options has emerged due to the theoretical, analytical and numerical advances in many aspects of libration mission design. In fact, the design strategies used for some spacecraft launched in the last years have been very successful, but much more challenging trajectories goals are already being suggested for the next few decades [7].

Within the last twenty years new analytical tools have been developed that provide approximations for many different solutions around the libration points in a number of dynamical models, and that include various types of periodic and quasi-periodic motions in their vicinity. The structure of the phase space in the vicinity of the collinear points has been studied and the fundamental motions determined, including the periodic halo orbits, as well as Lissajous trajectories and quasi-halos. The

capability to numerically and analytically produce these types of motion, for different dynamical models, in a fast and efficient way is an ongoing development. The local behaviour near these orbits is also of critical importance in any effort to develop general methodologies for mission analysis and has been the focus of several studies. These studies have been directly responsible for the application of invariant manifolds to ultimate produce viable nominal and transfer trajectories for several missions. Unique to upcoming missions are the designs of constrained transfer trajectories and mission orbits. They are designed to meet orbit goals for small Lissajous orbits, to minimise fuel and operational requirements and to provide formation or constellation options. Traditionally, libration orbit design has been analysed with a baseline trajectory concept set in place by project requirements or analytical boundary methods. That is, a trajectory had been base-lined so that science requirements are met. Future mission design requires a more generalised approach as operational considerations require the launch window, gravity assist, transfer trajectories, final orbits and the number of spacecraft to be as flexible as possible to optimise science return while minimising operational and launch requirements. As a consequence, and in order to satisfy the increasingly demanding requirements of libration point missions, it is desirable to have parametric descriptions of the trajectories around the libration points, together with their associated invariant manifolds, as global as possible. Moreover, trajectories for specific values of the parameters should be retrieved in a fast and simple way. We think that this will make easier and faster the choice of the suitable nominal and transfer trajectories for the mission designer. The development of methodology to fulfil these objectives is the main goal of the present paper.

The linear character of the flow around the collinear libration points of the Restricted Three Body Problem is centre $\times$ centre $\times$ saddle, so they have a 4–dimensional centre manifold in which lie all the nominal trajectories interesting for libration point missions. This centre manifold has 5–dimensional stable and unstable manifolds, made by the stable and unstable manifolds of its individual trajectories, which fill large neighbourhoods of the libration points in 6–dimensional space.

From these considerations follows that, when dealing with libration point orbits, we have to face with objects inside a high dimensional space, very difficult to be represented, wherein a four dimensional set of libration point orbits act as saddle points. To overcome the technical difficulties due to these facts, several mathematical tools have been developed up to present, and are essentially based in normal forms or in Lindstedt-Poincaré procedures. They pretend, in some way, to decrease the number of degrees of freedom as well as to decouple the hyperbolic parts from the elliptical ones, in order to simplify and study the problem from a mathematical point of view. They are one of the bases for the construction of new devices that permit mission analysis in a systematic way, avoiding trial and error strategies as much as possible.

Both methodologies, normal form and Lindstedt-Poincaré procedures, provide full descriptions of the orbits in selected energy levels. Nevertheless, they have several weak points. For instance, the energy level must be close to the one of the libration point, some of the variables used for the description of the flow do not have any physical meaning, the evaluation of the expansions can be time consuming, the change of variables from the usual position and velocity to amplitudes and phases must be implemented through iterative numerical procedures, etc.

Some of the drawbacks of the two above mentioned methodologies can be overcome by using numerical techniques for the computation of the families of periodic orbits and invariant tori of the centre manifold, as well as their invariant manifolds. The methodology for the computation of periodic orbits and their invariant manifolds is a classical one in simulation of dynamical systems. The computation of tori and their invariant manifolds is more recent and allows to obtain new families of invariant tori, apart from the well-known Lissajous orbits and quasi–halo orbits. Numerical techniques have a drawback on its own, which is that they produce individual trajectories but not parametrisations of families of trajectories. The combination of the best properties of each methodology, with an effec-

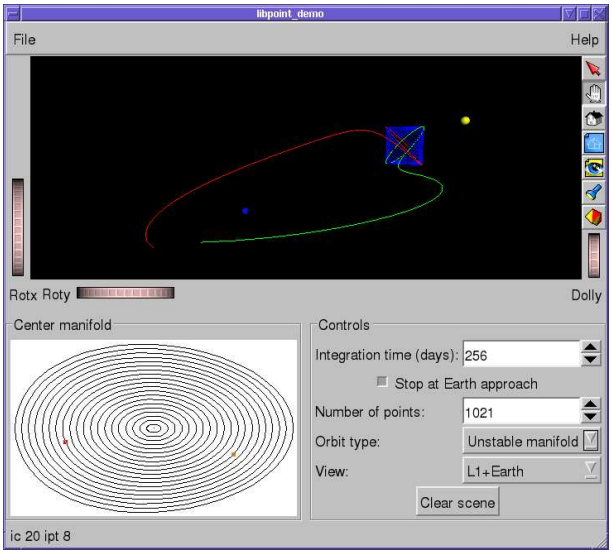

Fig. 1. Snapshot of a prototype of a possible gadget for the design of libration point trajectories.

tive implementation of the numerical procedures, is the basis for obtaining very efficient gadgets for mission design in the Solar System using libration points. A snapshot of a prototype of such a gadget, developed by our group in Barcelona, is shown in Fig. 1.

The goal of this paper is to show how to get in a fast and easy way the full set of orbits in a large energy range, together with their invariant stable and unstable manifolds, using an interpolation procedure over a sufficiently fine mesh of orbits. Section 2 is devoted to an overview of the methodology used for the computation and representation of libration point orbits. Section 3 contains the details of the computation of the mesh, interpolation and some characteristics of the Lissajous family of trajectories described. Section 4 is devoted to the refinement of a representative set of the computed orbits to a full Solar System model using JPL ephemerides.

2. COMPUTATION AND REPRESENTATION OF LIBRATION POINT ORBITS

The reference model that will be used is the circular restricted three body problem (CRTBP). As it is well known [10], this problem studies the behaviour of a particle with infinitesimal mass moving under the gravitational attraction of two primaries revolving around their centre of masses in circular orbits.

Using a suitable reference system and a dimensionless set of units, the equations of motion can be written as

$$\begin{aligned} \ddot{x}-2\dot{y} &= x-\frac{(1-\mu)}{r_1^3}(x-\mu)-\frac{\mu}{r_2^3}(x+1-\mu), \\ \ddot{y}+2\dot{x} &= y-\frac{(1-\mu)}{r_1^3}y-\frac{\mu}{r_2^3}y, \\ \ddot{z} &= -\frac{(1-\mu)}{r_1^3}z-\frac{\mu}{r_2^3}z, \end{aligned}$$

where $r_1=[(x-\mu)^2+y^2+z^2]^{\frac{1}{2}}$ and $r_2=[(x+1-\mu)^2+y^2+z^2]^{\frac{1}{2}}$ are the distances from the infinitesimal mass particle to the two primaries.

By introducing momenta as $p_x=\dot{x}-y$, $p_y=\dot{y}+x$ and $p_z=\dot{z}$, the equations of the CRTBP can be written in hamiltonian form with Hamiltonian function

$$H = \frac{1}{2}(p_x^2 + p_y^2 + p_z^2) - xp_y + yp_x - \frac{1-\mu}{r_1} - \frac{\mu}{r_2}.$$

The Hamiltonian is related to the well known Jacobi first integral through

$$C = -2H + \mu(1-\mu).$$

The above CRTBP equations have five equilibrium points, the so called libration points. Three of them, the collinear libration points, are in the line joining the primaries and they are usually denoted as L_1, L_2 and L_3. The other two are the triangular ones, and are in the plane of motion of the primaries forming an equilateral triangle with them. If x_{L_i} $(i = 1,2,3)$ denotes the abscissa of the three collinear points, we will assume that

$$x_{L_2} < \mu - 1 < x_{L_1} < \mu < x_{L_3},$$

and we will focus our attention in L_1.

The motion in the vicinity of the collinear equilibrium points can be seen as the composition of two oscillators and some "hyperbolic" behaviour. This means that the oscillations are not stable and that very small deviations will be amplified as time increases. One of the oscillations takes place in the plane of motion of the primaries and the other orthogonal to this plane. These two periodic motions are known as the planar and vertical Lyapunov periodic orbits. The frequencies of the oscillations vary with the amplitudes (since the problem is not linear), and for a suitable amplitude both frequencies become equal. At this point the well known halo–type periodic orbits appear. When the frequencies of the two oscillations (vertical and planar) are not commensurable, the motion is not periodic and it reminds a Lissajous orbit. Then we say that we have a quasi-periodic orbit. This kind of motion can be found both around the vertical periodic orbit and around the halo orbits.

A more synthetic way of displaying all this zoo of orbits consists in representing only their intersection with the $z = 0$ plane. This is what is usually called a Poincaré map representation. A planar orbit will appear as a closed curve on the plane and a quasi-periodic orbit as a set of points lying, more or less, on a smooth closed curve. Fig. 2 shows one of these representations. Near the centre of the figure one can see a fixed point. It corresponds to a vertical periodic orbit that crosses the $z = 0$ plane just at this point. It (and so, the corresponding orbit) is surrounded by quasi-periodic motions that take place on invariant tori. The external curve of the figure is the planar Lyapunov orbit (corresponding to a given value of the Jacobi constant). The two other fixed points are associated to the two halo orbits, which are symmetrical to one another with respect to $z = 0$. They are, in turn, surrounded by invariant 2D tori. Between the 2D tori around the vertical orbit and the ones around the halo orbit there is the trace of the stable and unstable manifolds of the planar Lyapunov orbit, which acts as a separatrix between two different kinds of motion: the ones around the vertical periodic orbits and the ones around the halo orbits.

Due to the unstable behaviour of the collinear libration points, this Poincaré map representation cannot be obtained by direct numerical integration of the CRTBP equations of motion. Fig. 2 was obtained after performing a normal form reduction of the Hamiltonian of the CRTBP and removing from the reduced Hamiltonian its unstable terms. Of course, this 2-dimensional figure corresponds to a fixed energy level (fixed value of the Jacobi constant or, equivalently, of the Hamiltonian). To get a global representation of the 4-dimensional central manifold around the libration point (recall that for the representation we have fixed the value of the z-coordinate equal to zero, which reduces in one unit the total dimension) we need to vary the value of the energy and for each energy level get the associated Poincaré map representation of the flow. This 3-dimensional picture can also be obtained by a more direct method. For this purpose we must compute the periodic orbits and invariant 2D tori

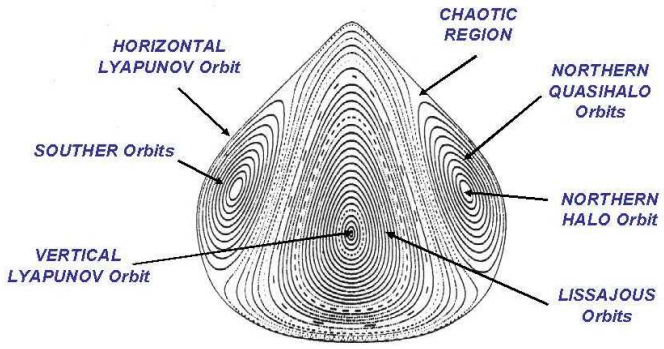

Fig. 2. Poincaré map representation of the orbits near the libration point L_1 for the value of the Jacobi constant 3.00078515837634. The CRTBP mass parameter corresponds to the Earth+Moon–Sun system.

of the centre manifolds of the libration points, using either Lindstedt-Poincaré or purely numerical procedures, and once they have been determined, represent their intersections with the $z = 0$ section for each energy level. To avoid the convergence problems of the Lindstedt-Poincaré method, we have selected numerical procedures.

2.1 Numerical computation of invariant tori

Numerical methods have been widely used in the past to compute fixed points and periodic orbits. The computation of invariant tori is not so extended. The procedure that has been used is based in the computation of the Fourier series of an invariant curve on the torus [5]. This strategy is combined with a multiple shooting procedure in order to deal with the unstable behaviour of the flow.
Consider a 2-dimensional invariant torus of the CRTBP with frequencies $\omega = (\omega_1, \omega_2) \in \mathbb{R}^2$. If ϕ_t denotes the flow associated to the CRTBP, a parametrisation $\Psi : \mathbb{T}^2 = [0, 2\pi]^2 \to \mathbb{R}^6$ of the torus satisfies the following invariant relation:

$$\Psi \begin{pmatrix} \xi + \omega_1 t \\ \eta + \omega_2 t \end{pmatrix} = \phi_t \left(\Psi \begin{pmatrix} \xi \\ \eta \end{pmatrix} \right), \qquad \text{for all} \quad \theta = (\xi, \eta) \in \mathbb{T}^2, \quad t \in \mathbb{R}. \tag{1}$$

Let us denote by T_i the period corresponding to the ω_i frequency, that is $T_i = 2\pi/\omega_i$. In order to reduce dimensions, instead of considering a parametrisation of the whole torus, we can consider the parametrisation of a curve in the torus which is invariant under ϕ_{T_2}. Such a curve is given by $\{\eta = \eta_0\}$, since from Eq. 1 we have

$$\Psi \begin{pmatrix} \xi + \omega_1 T_2 \\ \eta_0 \end{pmatrix} = \phi_{T_2} \left(\Psi \begin{pmatrix} \xi \\ \eta_0 \end{pmatrix} \right), \quad \text{for all} \quad \xi \in \mathbb{T}^1.$$

If $\varphi : \mathbb{T}^1 \to \mathbb{R}^n$ is the parametrisation of this curve, then we require

$$\varphi(\xi + \omega_1 T_2) = \phi_{T_2}\big(\varphi(\xi)\big), \quad \text{for all} \quad \xi \in \mathbb{T}^1, \tag{2}$$

where $\rho = \omega_1 T_2 = 2\pi\,\omega_1/\omega_2$ is the so called *rotation number* of the curve we are looking for. Note that the rotation number ρ uniquely identifies a torus at a given energy level.
The dynamical interpretation of the rotation number is clear: it represents the average variation of the angle ξ when the angle η has done one revolution, this is, has increased 2π units (see Fig. 3).
It is convenient to assume for φ a truncated Fourier series representation

$$\varphi(\xi) = A_0 + \sum_{k=1}^{N_f} \big(A_k \cos(k\xi) + B_k \sin(k\xi)\big), \tag{3}$$

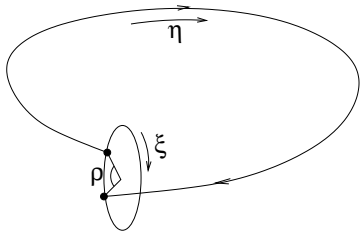

Fig. 3. Qualitative representation of the rotation number ρ.

in which the unknowns $A_k, B_k \in \mathbb{R}^n$ depend on the value of the energy h (given by the value of the Hamiltonian) and the rotation number ρ. Then, by taking $1+2N_f$ values of ξ, Eq. 2 can be turned into a finite–dimensional non–linear system of equations which can be solved for A_k, B_k. Concretely, we solve

$$\varphi(\xi_i+\rho) = \phi_{T_2}\big(\varphi(\xi_i)\big),$$

where $\xi_i = 2\pi/(1+2N_f)$ for $i = 0,\ldots,2N_f$. The error due to the truncation of the Fourier series of φ can be estimated by evaluating the invariance equation (Eq. 2) in phases not used in the discretisation, that is, for $\xi \neq \xi_i$. Namely, the error estimate can be taken as

$$\max_{\xi\in\mathbb{T}^1} \big\| \varphi(\xi+\rho) - \phi_{T_2}\big(\varphi(\xi)\big) \big\|_2. \tag{4}$$

Once we have a parametrisation of an invariant curve, a parametrisation of the whole torus can be recovered by numerical integration, as

$$\Psi(\xi,\eta) = \phi_{\frac{\eta}{2\pi}T_2}\Big(\varphi\big(\xi - \frac{\eta}{2\pi}\rho\big)\Big). \tag{5}$$

The details of the computational aspects (non–uniqueness of the Fourier representation, dealing with instability, actual implementation, computing effort, parallel strategies, etc.) of this procedure are given in [5].

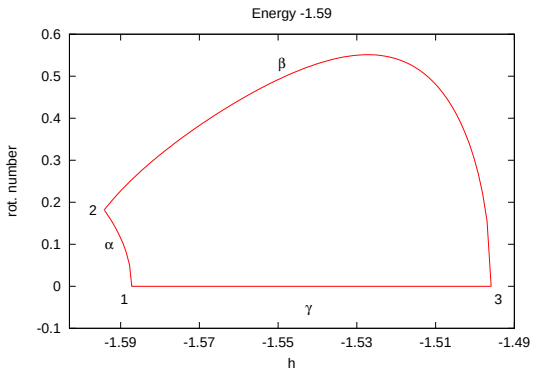

Fig. 4. Synthetic representation of the 2-parametric family of Lissajous orbits around the L_1 point, using as parameters the value of the Hamiltonian h and the rotation number ρ.

In Fig. 4 we have displayed, for the L_1 point the region, in the energy-rotation number plane, covered by the two-parametric family of tori computed starting from the vertical Lyapunov family of periodic orbits (Lissajous orbits) using the above mentioned procedure. In the (h,ρ) plane, the region of existence of Lissajous orbits shown in Fig. 4 is bounded by three different curves:

- The lower-left curve α (from vertex 1 to 2) is related to the planar Lyapunov family of periodic orbits. The orbits of this family represented in the curve are only those with central part, which are the only ones surrounded by tori. They are the "first" orbits of the family generated from the libration point.
- The upper piece β (from vertex 2 to 3) is strictly related to the vertical Lyapunov family of periodic orbits.
- The bottom boundary γ (from vertex 3 to 1) that corresponds to $\rho = 0$, begins at the value of the energy where the halo families are born. It is related to a separatrix between the tori around the vertical Lyapunov families and the halo ones.

Next, we can see how this synthetic representation of the 2-parameter family of Lissajous orbits is related to their Poincaré map representation at different energy levels. This is shown in Fig. 5. If in the (h,ρ) diagram we fix a value of the energy, we get a vertical segment connecting the β curve with the α or γ curve (depending on the value of h). For values of h lower than the one associated to the bifurcation of the halo families of periodic orbits (for instance, $h = -1.59$), the vertical segment connects β and α, which are associated, respectively, to the vertical and planar Lyapunov families of periodic orbits. This means that there is a 1-parameter family of Lissajous orbits (tori) connecting these two periodic orbits. The intersection of these Lissajous orbits with the $z = 0$ plane is displayed in the Poincaré map representation as a set of "concentric circles" with centre at the fixed point associated to the vertical periodic orbit and having as outer boundary the planar Lyapunov orbit. For any other value of h the vertical segment in the (h,ρ) goes from the β curve, associated to the vertical Lyapunov family, to the γ curve, for which $\rho = 0$. As it has been said, this last curve represents the separatrix between the tori around the vertical Lyapunov families and the halo ones, so now the 1-parameter family of Lissajous orbits will start also close to the vertical Lyapunov periodic orbit and will have a natural termination when it reaches the separatrix. The intersection of these Lissajous orbits with $z = 0$ are the closed curves around the central fixed point in the Poincaré map representation.

2.2 Numerical computation of invariant stable/unstable manifolds

The numerical computation of the stable/unstable manifolds of periodic orbits is easy using their linear approximation given by the hyperbolic eigenvectors of the monodromy matrix. For invariant tori the situation, although similar, is not trivial. In our computations we have used the procedure introduced in [6]. The basic idea is the following: assume that $\xi \to \varphi(\xi)$ parametrises an invariant curve on a torus satisfying the invariant relation

$$\varphi(\xi + \omega_1 T_2) = \phi_{T_2}\big(\varphi(\xi)\big).$$

Now, for each value of ξ we are looking for a 2π–periodic function $v : \mathbb{R} \to \mathbb{R}^6$ giving the linear approximation of the stable/unstable manifold at $\varphi(\xi)$, this is

$$D\phi_{T_2}\big(\varphi(\xi)\big)v(\xi) = \Lambda v(\xi + \omega_1 T_2) = \Lambda v(\xi + \rho),$$

for a certain Λ which is called, analogously to the case of periodic orbits, characteristic multiplier. Also, if $\Lambda > 1$ we get the unstable direction and if $\Lambda < 1$ the stable one. To find solutions of the above equation, first we rewrite it as

$$D\phi_{T_2}\big(\varphi(\xi - \rho)\big)v(\xi - \rho) = \Lambda v(\xi). \tag{6}$$

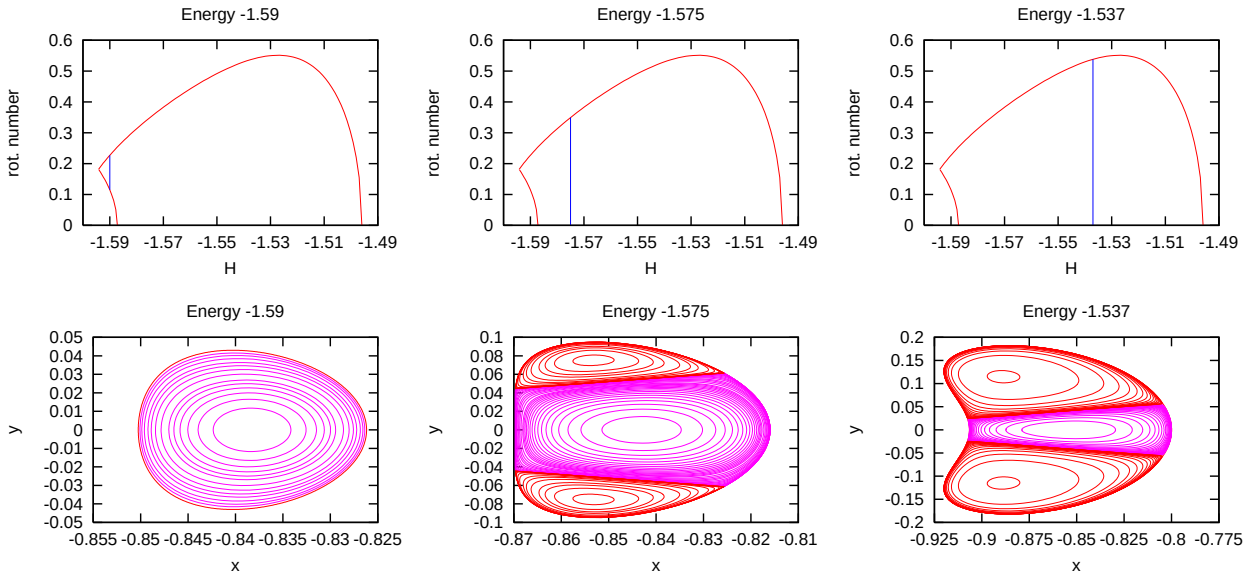

Fig. 5. Two synthetic representations of the 2-parametric family of Lissajous orbits around the L_1 point. In each (h,ρ) representation, the vertical (blue) line represents the family of Lissajous orbits around the vertical periodic orbit with a fixed value of the energy. In the Poincaré map representation, which is displayed below, these Lissajous orbits are represented by their intersection with $z=0$ and are the closed curves in the centre of each plot coloured in magenta, around the central fixed point associated to the vertical periodic orbits. The red curves of the Poincaré maps correspond to the quasi–halo family of invariant tori and are given for completeness. They are not related to the h–ρ diagrams of the first row.

The use of finite Fourier expansions allows to transform Eq. 6 into a finite–dimensional eigenvalue problem,

$$M\boldsymbol{c} = \Lambda \boldsymbol{c}, \tag{7}$$

where $\boldsymbol{c}$ is the vector of Fourier coefficients of $v(\xi)$, and M is a suitable (finite) matrix. Some details on the construction of the M matrix can be found in [9]. The error due to the truncation of the Fourier series of $v(\xi)$ again can be estimated using the invariance equation (Eq. 6). Namely, we can take as error estimate

$$\max_{\xi\in\mathbb{T}^1} \left\| D\phi_{T_2}\big(\varphi(\xi-\rho)\big)v(\xi-\rho) - \Lambda v(\xi)\right\|_2. \tag{8}$$

The eigenvalues of the discretised equation (Eq. 7) appear grouped in circles. If the torus is reducible, this is, the linear variational equations with quasi-periodic coefficients can be reduced to constant coefficients, then there are as many circles as eigenvalues of the reduced monodromy matrix and each circle contains one of them. In our case, due to the Hamiltonian character of the CRTBP, we have four unit circles and two additional circles containing Λ and Λ^{-1} for some $\Lambda > 1$. The associated eigenvectors $v_\Lambda(\xi)$ and $v_{\Lambda^{-1}}(\xi)$ give the linear approximation of the unstable/stable manifolds.
Once we have the linear approximation of the invariant manifolds associated to an invariant curve of the torus, we can globalise it using

$$v(\xi,\eta) = \Lambda^{-\eta/2\pi} D\phi_{\frac{\eta T_2}{2\pi}}\left(\varphi(\xi - \frac{\eta}{2\pi}\rho)\right) v(\xi - \frac{\eta}{2\pi}\rho).$$

In Fig. 6 we show the 3D unstable manifold associated to a Lissajous orbit around L_1 for different values of η when $\xi \in [0, 2\pi]$.

3. GLOBAL DESCRIPTION OF THE LISSAJOUS FAMILY

The numerical methods outlined in last section allow to compute individual trajectories. By applying

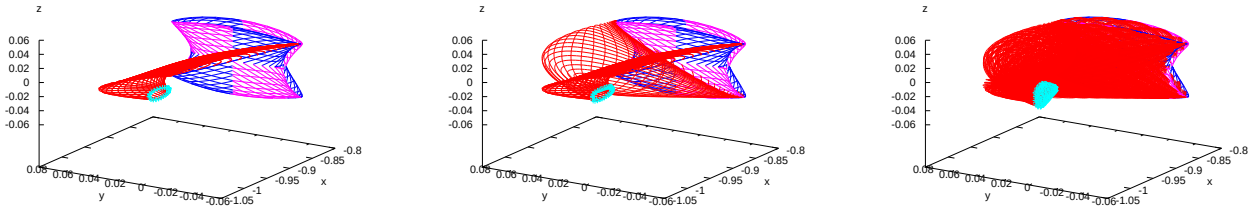

Fig. 6. From left to right, unstable manifold associated to a Lissajous orbit at: $\eta = 0$, $\eta = 0, \pi$ and at 15 different values of η equally spaced in $[0, 2\pi]$.

continuation methods, one–parametric families of tori can be followed. For the case of tori around Lyapunov periodic orbits, any value of h, ρ can be reached by continuation, but this can be a rather time–consuming process. A fast way to obtain trajectories for any h, ρ is to interpolate between previously computed ones, provided they are part of a mesh fine enough for the interpolation to be accurate. This section is devoted to the presentation of results related to the implementation of this strategy.

A grid of invariant tori covering the (h, ρ) region of Lissajous orbits around L_1 for the Earth–Moon mass ratio (see Fig. 4) has been computed by numerical continuation with respect to h of several one–parametric families of tori with constant rotation number, starting from Lyapunov vertical and planar periodic orbits with energy smaller than the maximum of the curve β in Fig. 4. A total of 220 families have been continued, corresponding to an approximately uniform[1] spacing of ρ of 0.0025 units. During the continuation of each family, Fourier series of tori have been stored for equally spaced values of h, with a spacing of 0.0005 units. The number of harmonics N_f has been increased as needed in order to obtain the error estimate of Eq. 4 smaller that 10^{-10} (3.85×10^{-5} km). The continuations have been stopped when the N_f has reached a maximum allowed value of 100 harmonics. The spacing in h and ρ used has been empirically determined in order to obtain an interpolation error of about 10^{-10} in most of the (h, ρ) region (see below). The computed grid of tori consists of a total of 25433 Fourier series of invariant curves, each one also with the error estimate of Eq. 4 smaller than 10^{-10}. The corresponding grids of invariant stable and unstable manifolds have been computed by solving the eigenvalue problem of Eq. 7 for each of the parametrisations φ of the grid of invariant tori. Some additional details about execution time and storage requirements can be found in [9].

In order to estimate the interpolation error on the region covered by the computed grids of tori and manifolds, the error estimates of Eqs. 4,8 have been evaluated on the Fourier series obtained by interpolation at the midpoints of the grids. The results are show in Figs. 7,8.

Fig. 7 shows that, in the case of tori, interpolation error ranges between 10^{-10} and 10^{-8} for most of the region. It increases in three different zones:

(a) Near the planar and vertical Lyapunov families of periodic orbits, this is, near the α and β curves of Fig. 4.

(b) In some horizontal strips, which correspond to resonances between the planar and vertical frequencies of the computed tori. From top to bottom, they correspond to the values $\rho = 2\pi/13, 2\pi/15, 2\pi/17, \ldots$

[1] The rotation numbers have been "Diophantised" in order to be far from low–order resonances. See [5] for more details.

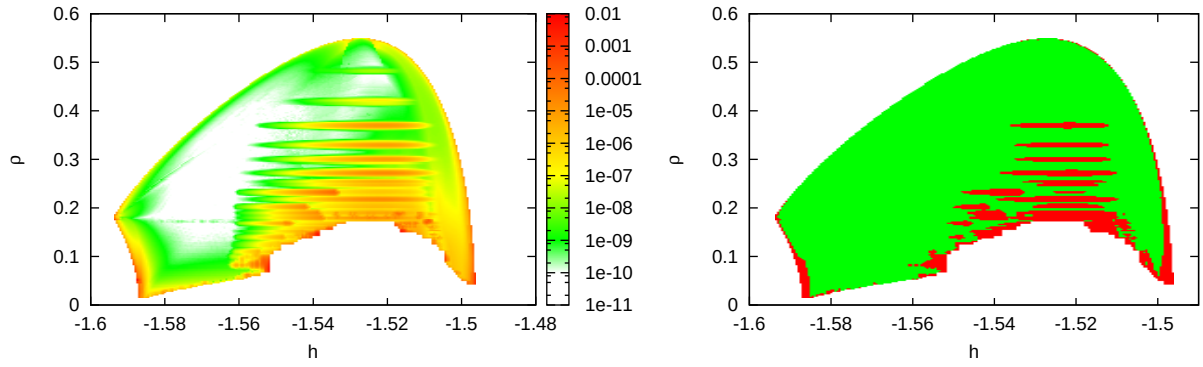

Fig. 7. Interpolation error on the midpoints of the grid of tori. Left: value of the estimate of Eq. 4. Right: interpolated tori with error estimate smaller than 10^{-6} (green), and larger than this value (red).

(c) Near the bottom of the region, this is, the γ curve of Fig. 4, which corresponds to the separatrix between quasi–periodic motions around Lyapunov vertical and halo periodic orbits.

In the (c) case it is natural to expect an increasing interpolation error, since it corresponds to the stopping of the continuation process during the computation of the grid, either by computational limit (reaching the maximum allowed value of N_f) or by breakdown of tori close to the separatrix.[2] For the (a) case, a refinement of the grid (recall that it is regularly spaced in h, ρ) is expected to decrease the interpolation error, since the grid points in the corresponding (h, ρ) zones have the error estimate of Eq. 4 smaller than 10^{-10}. The (c) is also natural, as low–order resonances dynamically play a role (for instance, the 1:17 resonance, corresponding to the $\rho = 2\pi/17$ strip, can be observed in Fig. 2 as an island chain). If high accuracy is needed, these resonant orbits should be computed as different families, as has been done in [5] for the quasi–halo case.

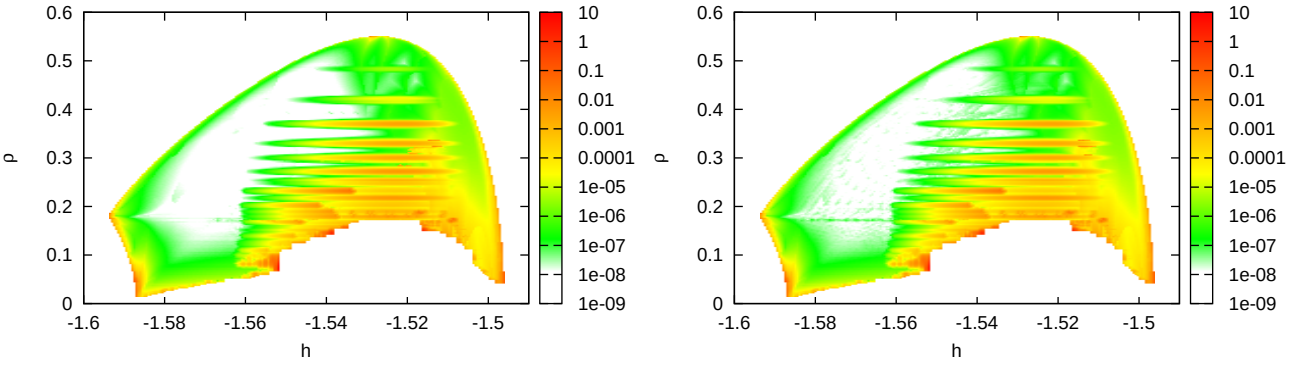

Fig. 8. Relative interpolation error on the midpoints of the grid of unstable (left) and stable (right) manifolds.

Fig. 8 shows the results corresponding to the evaluation of a relative error version of the estimate of Eq. 8,

$$\max_{\xi \in \mathbb{T}^1} \frac{\left\| D\phi_{T_2}\left(\varphi(\xi-\rho)\right) v(\xi-\rho) - \Lambda v(\xi) \right\|_2}{\|\Lambda v(\xi)\|_2},$$

on the midpoints of the grids of unstable and stable manifolds. It is seen that the error has the same qualitative behaviour as the error for tori shown in Fig. 7.

In order to have an idea of the size of the orbits considered, Fig. 9 displays the behaviour of the size (in km) of the Lissajous invariant tori in terms of h, ρ. Only the midpoints of the grid of tori with

[2] This is a common phenomenon in Hamiltonian systems and is predicted by KAM theory.

interpolation error smaller than 10^{-6} (see Fig. 7 right) have been considered. For each torus, the maximum difference between the x, y, and z coordinates has been computed, by taking 128 equally spaced values of ξ and η in Eq. 5. It can be observed that, for constant ρ and increasing energies, the x and y amplitudes are non–monotonous, due to the fact that the corresponding one–parametric sub-families end at vertical Lyapunov periodic orbits (the β curve in Fig. 4), which have no planar amplitude. On the other hand, the z amplitude is always increasing with energy for constant ρ.

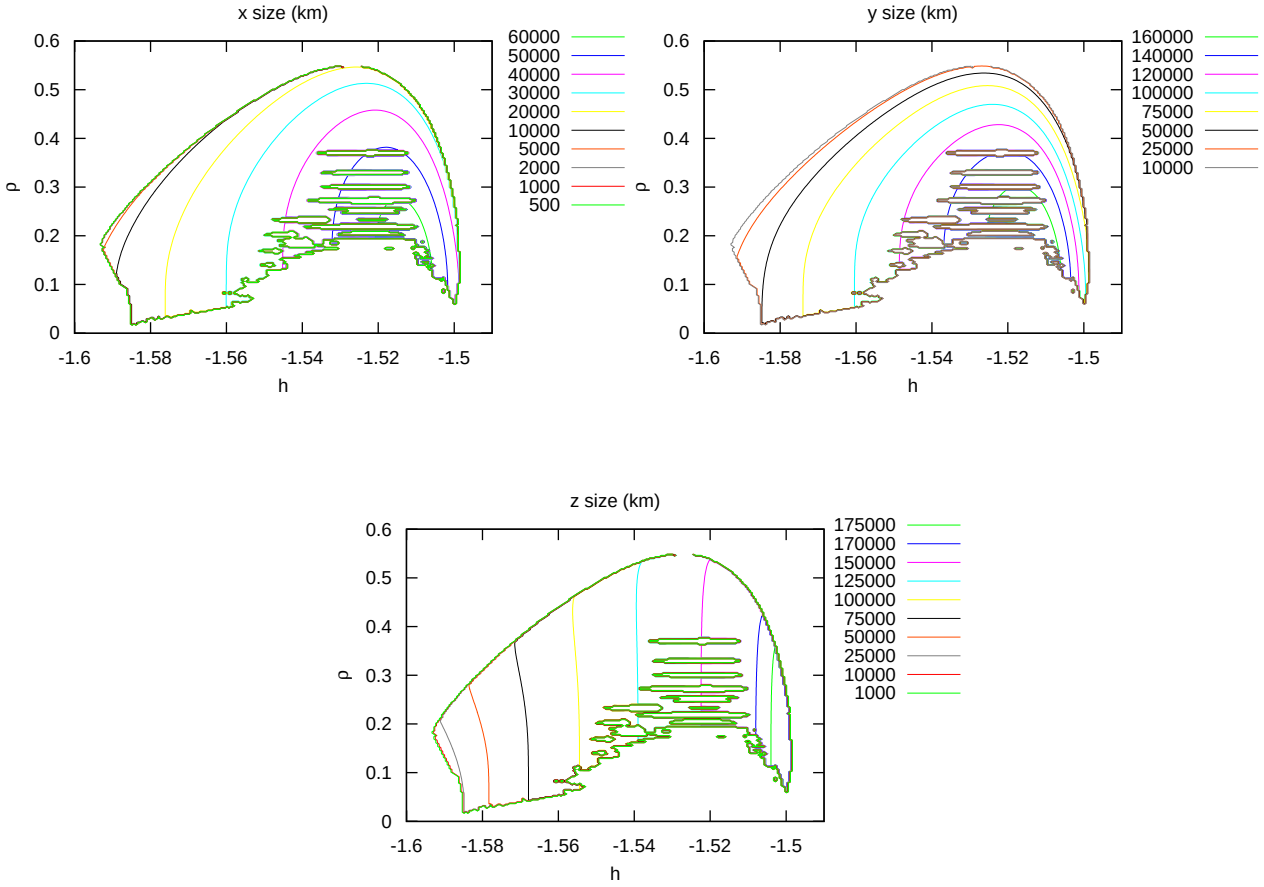

Fig. 9. Diagrams h–ρ displaying as level curves the size in the x, y and z coordinates the 2D tori of the Lissajous family around L_1 (for the Earth–Moon mass ratio). The units for size are km.

4. NUMERICAL REFINEMENT

In order to illustrate the usefulness as actual spacecraft trajectories of the interpolated Lissajous families of the previous Section, we have proceeded to their numerical refinement into a N-body model, in which the N bodies are the Sun and the planets of the solar system, whose positions and velocities are provided by the JPL ephemerides (DE403).

For the refinement, we have used an unconstrained multiple shooting method, taking as initial seed a certain number of nodes computed using the interpolated orbit (determinated in the CRTBP vector-field). The Lissajous orbits are around the collinear equilibrium point L_1 of the Earth-Moon system. The values of the energy h and rotation number ρ of these orbits are displayed in Fig. 10.

In the range of admissible parameters (h, ρ) displayed in the above figure, we have selected 1100 uniformly distributed pairs and for each pair we have determined, by interpolation, the associated Lissajous orbit. These are the orbits used for the numerical refinement.

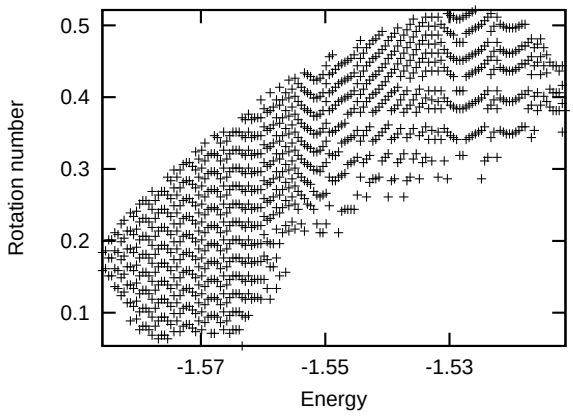

Fig. 10. The black points represent the values of the energy and rotation number of the Lissajous orbits around the libration point L_1 of the Earth-Moon system used for refinement.

4.1 The multiple shooting method

Since the refined solutions are computed numerically, and the equations of motion are time dependent, an initial epoch and a fixed time span must be selected. The refined orbit will be computed for the time interval defined by these two quantities.

As in the standard multiple shooting method, the total time span is split into a number of shorter subintervals selecting, for instance, N equally spaced points $t_1, t_2, ..., t_N$ (t_1 is the initial epoch and $t_N - t_1$ the length of the time interval mentioned above). Denote by $\Delta t = t_{i+1} - t_i$ and by

$$Q_i = (t_i, x_i, y_i, z_i, \dot{x}_i, \dot{y}_i, \dot{z}_i,)^T, \quad i = 1, 2, ..., N,$$

the points on a Lissajous orbit of the CRTBP, equally spaced (Δt) in time. Let $\phi(Q_i)$ be the image of the point Q_i under the flow associated to the equations of motion in the N-body model after an amount of time Δt. As, in this way, the epochs t_i are fixed, we can write $Q_i = (x_i, y_i, z_i, \dot{x}_i, \dot{y}_i, \dot{z}_i,)^T$. If all the points Q_i were on the same orbit of the new vector-field, then $\phi(Q_i) = Q_{i+1}$ for $i = 1, ..., N-1$. As this is not the case, a change of the starting values is needed in order to fulfil the matching conditions. In this way, one must solve (using Newton's method) a set of $N-1$ nonlinear equations, which can be written as

$$F \begin{pmatrix} Q_1 \\ Q_2 \\ \vdots \\ Q_N \end{pmatrix} = \begin{pmatrix} \phi(Q_1) \\ \phi(Q_2) \\ \vdots \\ \phi(Q_{N-1}) \end{pmatrix} - \begin{pmatrix} Q_2 \\ Q_3 \\ \vdots \\ Q_N \end{pmatrix} = \Phi \begin{pmatrix} Q_1 \\ Q_2 \\ \vdots \\ Q_{N-1} \end{pmatrix} - \begin{pmatrix} Q_2 \\ Q_3 \\ \vdots \\ Q_N \end{pmatrix} = 0.$$

If $Q^{(j)} = \left(Q_1^{(j)}, Q_2^{(j)}, ..., Q_N^{(j)}\right)^T$, denotes the j-th iterate of the procedure, Newton's equations can be written as

$$DF(Q^{(j)}) \cdot (Q^{(j+1)} - Q^{(j)}) = -F(Q^{(j)}),$$

where the differential of the function F has the following structure

$$DF = \begin{pmatrix} A_1 & -I & & \\ & A_2 & -I & \\ & & \ddots & \ddots \\ & & & A_{N-1} & -I \end{pmatrix},$$

with $D\Phi = \mathrm{diag}(A_1, A_2, ..., A_{N-1})$. As each of the transition matrices, A_i, that appear in $D\Phi$ are 6×6, at each step of the method we have to solve a system of $(N-1) \times 6$ equations with $6 \times N$ unknowns, so some additional conditions must be added. This is the only difference with the standard multiple shooting method and is due to the fact that our problem is not a real boundary-value one. As additional equations we could fix some initial and final conditions at $t = t_0$ and $t = t_N$. In this case one must take care with the choice because the problem can be ill conditioned from the numerical point of view. This is because the matrix $DF(Q)$ can have a very large condition number. To avoid this bad conditioning, we can choose a small value for Δt, but in this case, as the number of points Q_i increases (if we want to cover the same time span) the instability is transfered to the procedure for solving the linear system. Also, the extra boundary conditions can force the solution in a non natural way giving convergence problems when we try to compute the orbit for a long time interval.
To avoid this, we can apply Newton's method directly. As the system has more unknowns than equations, we have (in general) an hyper-plane of solutions. From this set of solutions we try to select the one closest to the initial orbit used to start the procedure. This is done by requiring the correction to be minimum with respect to some norm (i.e. the Euclidean norm). The use of the normal equations must be avoided because they are usually ill conditioned too. More precisely, denoting by $\Delta Q^{(j)}$

$$\Delta Q^{(j)} = Q^{(j+1)} - Q^{(j)},$$

requiring $\|\Delta Q^{(j)}\|_2$ to be minimum, one gets the Lagrange function $L(\Delta Q, \mu)$ with (vector) multiplier μ

$$L(\Delta Q, \mu) = \Delta Q^T \cdot \Delta Q + \mu^T \cdot (F(Q) + DF(Q) \cdot \Delta Q),$$

we get

$$\Delta Q^{(j)} = -DF(Q^{(j)})^T \cdot \left[DF(Q^{(j)}) \cdot DF(Q^{(j)})^T \right]^{-1} \cdot F(Q^{(j)}), \tag{9}$$

which gives the value of $\Delta Q^{(j)}$ explicitly. However since the matrix $DF(Q^{(j)})$ is usually very big, a special factorisation in blocks is suitable to get the solution of Eq. 9 in a computationally and efficient way. See [4] for the implementation and the properties of the algorithm and [1] for a multiple shooting procedure with constraints in the variations of the nodes.

4.2 Numerical results

Using the multiple shooting procedure explained in the above section, we have proceeded to the numerical refinement of a large set of Lissajous orbits around the L_1 point of the Earth-Moon system. The procedure is started using as initial nodes Q_i equally spaced points (in time) of the interpolated Lissajous orbits. The initial epoch for the JPL ephemerides has been fixed to be January 1 2000. The number of nodes, the value of $\Delta t = t_{i+1} - t_i$ between two consecutive nodes and the total time interval $t_N - t_1$ (in dimensionless CRTBP units) are given in Table 1.

No. nodes	Δt	Total t
600	$\pi/100$	6π
800	$\pi/100$	8π

Table 1. Values of the parameters used for the numerical refinement.

The iterative procedure finishes when the value of the norm of the error function or of the correction is less than a certain threshold ($5 \cdot 10^{-7}$ and $1 \cdot 10^{-6}$, respectively) or the number of iterations exceeds a fixed amount (20). In Fig. 11 we show the number of iterations required, as well as the value of the norm of the error in the last iteration, for the three sets of parameters used for the refinement. Clearly,

for fixed thresholds, the number of iterations increases either with the total time interval and with the value of Δt, but there are not relevant variations when moving within the family of Lissajous orbits.

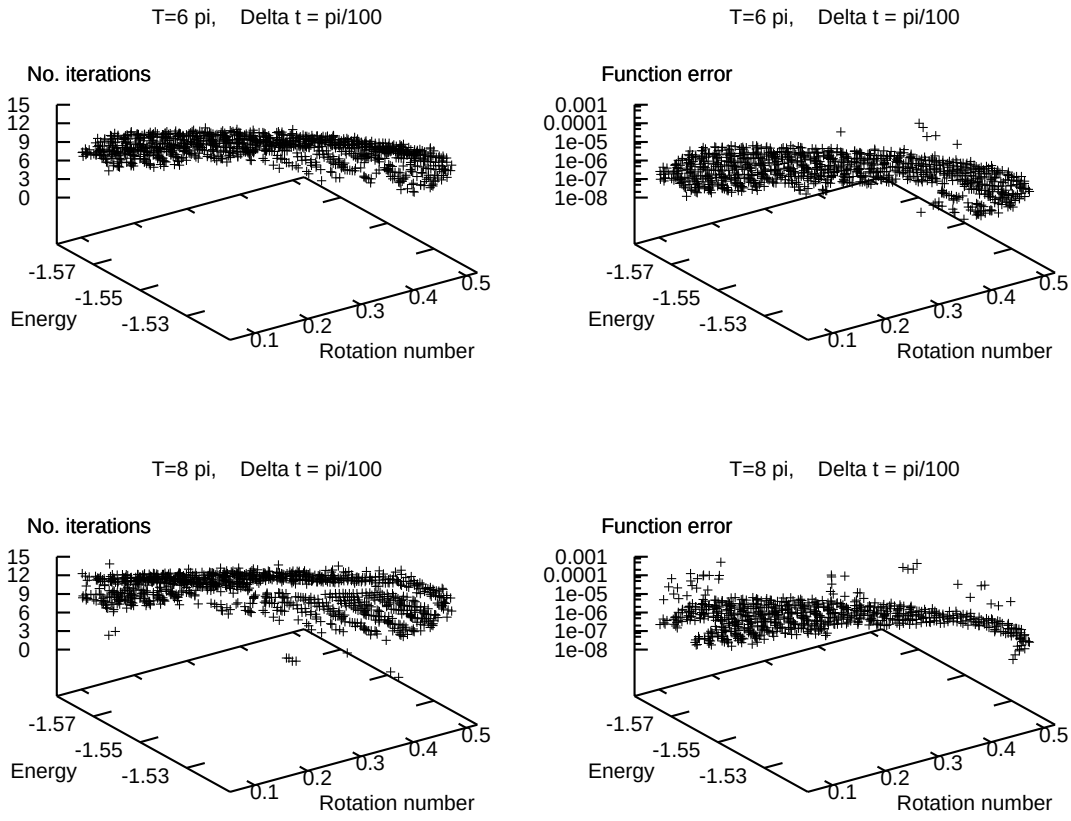

Fig. 11. Behaviour of the number of iterations required for the refinement (left plots) and the norm of the error after the last iteration for the family of Lissajous orbits considered. The number of nodes and Δt values are (600, $\pi/100$) for the first row, and (800, $\pi/100$) for the second row.

5. CONCLUSIONS AND OUTLOOK

In this paper, it has been shown how to apply numerical techniques to accurately compute libration point orbits (tori) and their stable and unstable manifolds. An interpolation procedure has been designed, which allows to parametrically describe families of libration point orbits and their invariant manifolds in a global way. This procedure has been illustrated for the L_1 point, Earth–Moon mass ratio, with the computation a fine grid of Lissajous trajectories, as well as their corresponding invariant manifolds. An application has been made to the refinement of a representative set of trajectories to a full Solar System model.

6. ACKNOWLEDGEMENTS

This work has been partially supported by the Spanish grants MTM2006-05849/Consolider (E.B., G.G., J.M.M.), MTM2008-01486 (J.M.M.), MTM2009-06973 (M.O.), and the Catalan grants 2009-SGR410 (J.M.M.), 2009-SGR859 (M.O.). The numerical explorations have been carried out in the Beowulf clusters Antz (Universitat Autònoma de Barcelona) and Hidra (Universitat de Barcelona).

REFERENCES

[1] E. Alessi, G. Gómez, and J. Masdemont. Transfer Orbits in the Earth–Moon System and Refinement to JPL Ephemerides. Proceedings of the ISSFD conference, 2009.

[2] E. Canalias, G. Gómez, M. Marcote, and J. Masdemont. Assessment of Mission Design Including Utilization of Libration Points and Weak Stability Boundaries. *ESA Advanced Concept Team*, URL: http://www.esa.int/gsp/act/publications/pub-mad.htm, 2004.

[3] D. Dunham and R. Farquhar. Libration Point Missions, 1978–2002. In G. Gómez, M. Lo, and J. Masdemont, editors, *Libration Point Orbits and Applications*, pages 45–73, 2003.

[4] G. Gómez, J. Masdemont, and C. Simó. Quasihalo Orbits Associated with Libration Points. *Journal of The Astronautical Sciences*, 46(2):1–42, 1999.

[5] G. Gómez and J. Mondelo. The Dynamics Around the Collinear Equilibrium Points of the RTBP. *Physica D*, 157(4):283–321, 2001.

[6] A. Jorba. Numerical computation of the normal behaviour of invariant curves of n–dimensional maps. *Nonlinearity*, 14:943–976, 2001.

[7] W. Koon, M. Lo, J. Marsden, and S. Ross. Constructing a low energy transfer between jovian moons. *Contemporary Mathematics*, 292:129–145, 2002.

[8] M. Lo, B. Williams, W. Bollman, D. Han, Y. Hahn, J. Bell, E. Hirst, R. Corwin, P. Hong, K. Howell, B. Barden, and R. Wilson. Genesis Mission Design. *The Journal of the Astronautical Sciences*, 49:169–184, 2001.

[9] J. M. Mondelo, E. Barrabés, G. Gómez, and M. Ollé. Numerical parametrizations of Libration Point trajectories and their invariant manifolds. *Advances in the Astronautical Sciences*, 129:1153–1168, 2008.

[10] V. Szebehely. *Theory of Orbits*. Academic Press, 1967.

◄ BACK TO SESSION DETAILED CONTENTS ◄ BACK TO HIGHER LEVEL CONTENTS